Influence of Peruvian Flat-Subduction Dynamics on the Evolution of Western Amazonia

Caroline M. Eakin[1*], Carolina Lithgow-Bertelloni[2], and Federico M. Dávila[2,3]

[1]*Department of Geology and Geophysics, Yale University, New Haven, CT 06520, USA*

[2] *Department of Earth Sciences, University College London, London, UK*

[3]*CICTERRA-CONICET and Universidad Nacional de Córdoba, Córdoba, Argentina*

[*]*Corresponding Author*:

Caroline M. Eakin

caroline.eakin@yale.edu

Department of Geology and Geophysics, Yale University, New Haven, CT 06520, USA

Phone: +15107178942

ABSTRACT

Convection in the Earth's mantle is mainly driven by cold, dense subducting slabs, but relatively little is known about how 3D variations in slab morphology and buoyancy affect mantle flow or how the surface above deforms in response (i.e. dynamic topography). We investigate this problem by studying the dynamics of an active region of flat-slab subduction located in Peru in South America. Here the slab geometry is well known, based on the regional seismicity, and we have observations from the local geological record to validate our models. Of particular interest is the widespread subsidence and deposition of the Solimões Formation across western Amazonia that

coincided with the development of the Peruvian flat-slab during the Mid-Late Miocene. This formation covers an extensive area from the foredeep to the Purus Arch located ~2000 km away from the trench. Close to the Andes the preservation of several kilometers of sedimentary thicknesses can be easily accounted for by flexure. Based on an estimate of the Andean loading we predict 2.8 to 3.6 km of accommodation space that spans 100 km. The spatial and temporal history of the Solimões Formation however, particularly the thick distal foreland accumulations up to 1.2 km deep, can only be matched with the addition of a longer-wavelength dynamic source of topography. Following the transition from normal to flat subduction, we predict over 1 km of dynamic subsidence (~1500 km wide) that propagates over 1000 km away from the trench, tracking the subduction leading edge. This is followed by a pulse of dynamic uplift over the flat segment behind it. We therefore propose that a combination of uplift, flexure and dynamic topography during slab flattening in Peru is responsible for the sedimentation history and landscape evolution of western Amazonia that eventually led to the configuration of the Amazon Drainage Basin we know today.

KEYWORDS

Dynamic Topography; Flat-Slab Subduction; Amazonia; Solimões Formation;

1. INTRODUCTION

Subducting slabs represent the primary buoyancy force in Earth's mantle and a critical source of surface deformation via their coupling to the overriding plate. Yet the impact of variations in slab morphology and buoyancy (e.g. slab tears or the subduction

of oceanic plateaus) on the dynamics of the mantle and how the upper plate deforms in response are poorly understood. The importance of such along strike variability in subduction models is however becoming increasingly apparent (e.g. Guillaume et al., 2009; Dávila and Lithgow-Bertelloni, 2013; Capitanio and Faccenda, 2012; Jadamec et al. 2013). Of particular concern are episodes of "flat" or "shallow" subduction that represent 10% of subduction zones worldwide today (Gutscher et al., 2000b), and often invoked to account for widespread deformation in continental interiors, such as for the western US during the Laramide orogeny (Dickinson and Snyder, 1978; Bird, 1988).

1.1 Tectonic and Geological Setting

The Peruvian subduction zone presents itself as an excellent modern-day natural laboratory to study the interaction between this flat-subduction and surface deformation. Extending over 1500 km along strike, the Peruvian flat-slab segment (3 °S to 15 °S) is by far the most extensive region of flat subduction in the world (Fig. 1). The slab subducts at a normal dip (~ 40°) to a depth of around 100 km, most likely directly beneath the over-riding continental lithosphere, and travels horizontally for several hundred kilometers before steepening again to the east (Cahill and Isacks, 1992; Phillips and Clayton, 2014). The region is characterized by a distinct lack of contemporary arc volcanism and low heat flow (~20 mW/m^2) (Henry and Pollack, 1988), in contrast to the normally dipping (~30°) regions to the north and south.

Subduction has been operating along the western coast of Peru since at least the Jurassic (Martinod et al., 2010), with the present plate configuration stable since 23 Ma, following the formation of the Nazca and Cocos plates (Lonsdale, 2005). The presence of

69 the Peruvian flat-slab is however relatively recent in comparison. Although the precise
70 date is unclear and is still a matter of debate, slab flattening is likely to have started
71 around the Mid to Late Miocene (Bissig et al., 2008; Ramos and Folguera, 2009) around
72 the time when the Nazca Ridge first reached the trench (~ 11-15 Ma: Hampel, 2002;
73 Rosenbaum et al., 2005) and the pattern of arc volcanism began to change (Aleman,
74 2006; Bissig et al., 2008). Full flat-slab development is likely a long process that can last
75 from several to 10 Myr (Arrial and Billen, 2013; Espurt et al., 2008; Martinod et al.,
76 2010; van Hunen et al., 2002a; 2002b). The various stages of progression include
77 broadening of the volcanic arc and crustal deformation, adakitic magmatism, thinning
78 and cooling of the asthenospheric wedge resulting in a decline and eventual cessation of
79 volcanic activity (Gutscher et al., 2000a). Over central Peru there is evidence that the arc
80 broadened around 11-12 Ma (Aleman, 2006; Bissig et al., 2008; Ramos and Folguera,
81 2009), that adakites formed 3-6 Ma (Gutscher et al., 2000a) and that magmatic activity
82 ended by 3-4 Ma (Soler and Bonhomme, 1990; Rosenbaum et al., 2005; Pilger, 1981;
83 Espurt et al., 2008; Martinod et al., 2010).

84 Whilst shallow subduction was beginning to take hold beneath Peru, the surface
85 above was also going through its own transformation. Eventually this transformation
86 would lead to the development of the largest drainage basin in the world, the Amazon
87 River system, and the most diverse habitat on the planet, the Amazon Rainforest.
88 Initially, during the Early-Mid Miocene, it has been suggested that regional drainage of
89 Amazonia escaped towards the north into the Caribbean Sea (e.g. Hoorn et al., 1995), or
90 exited towards the west through the Guayaquil gap into the Pacific Ocean (e.g. Potter,
91 1997), as the Andes had not yet grown into a full orogenic barrier. During the Late

92 Miocene however, the northern Andes rose rapidly, shutting off drainage pathways to the
93 north and west, and deepening and broadening the foreland basins to the east (Jordan and
94 Gardeweg, 1989; Kroonenberg et al., 1990; Hoorn et al., 1995; 2010; Nobret et al., 1996;
95 Garzione et al., 2008). At the same time, a wide but relatively shallow subsiding system
96 developed in western Amazonia, from eastern Peru to the Purus Arch (Fig. 1),
97 represented by the Solimões/Pebas Formation (Hoorn, 1993; 1994; Campbell et al., 2006;
98 Wesselingh et al., 2006b; Gross et al., 2011; Latrubesse et al., 2010; Rodrigues Nogueira
99 et al., 2013). Deposition of this Solimões Formation ceased in the Mio-Pliocene, as the
100 accumulation rate of terrigenous material on the offshore Amazon fan increased
101 dramatically (Dobson et al., 2001; Latrubesse et al., 2010). This indicated a switch in the
102 destination of the bulk of Andean derived sediment, from deposition in the western
103 Amazonian basins, to large-scale transportation across the continent via a fully fledged
104 Amazon River to the Atlantic margin (Campbell et al., 2006; Figueiredo et al., 2009;
105 Latrubesse et al., 2010).

106 At the time of deposition, the Solimões Formation recorded a wide area of
107 subsidence that resulted in simultaneous partial infilling of many different pre-existing
108 sub-basins in the western Amazonian region (labeled in Fig. 1), both foreland (e.g. Madre
109 de Dios) and intra-cratonic (e.g. Solimões) (Hoorn, 1994). The E-W trending series of
110 Acre, Solimões, and Amazonas basins overlie the Amazonian Craton subdividing the
111 craton's exposure at the surface into the northern Guyana and southern Brazilian Shields
112 (Fig. 1), the result of an extensional event during the Mid-Proterozoic (Wanderley-Filho
113 et al., 2010). Following on during the Late-Proterozoic some of the original extensional
114 grabens were positively inverted to form basement arches which now separate the

115 individual sub-basins, for example the Purus Arch which partitions the Solimões basin
116 from the Amazonas basin and is the eastern limit of the Solimões Formation, was an
117 inversion of the Cachimbo Graben (Wanderley-Filho and Costa, 1991). These
118 Precambrian structural highs have therefore played an important role in sub-division and
119 configuration of sedimentary deposits across western Amazonia ever since.
120
121 **1.2 Sources of Topography and their Effect upon the Landscape**
122 The evolving landscape and drainage of lowland Amazonia has typically been
123 attributed to interaction of climate, sea level and the developing Andean mountain belt. In
124 particular the intense period of uplift during the Miocene is thought to have increased
125 erosional rates, sediment fluxes, and the deformation of inland Amazonia via flexural
126 processes (Hoorn et al., 1995; 2010a; 2010b; Figueiredo et al., 2009; Mora et al., 2010;
127 Latrubesse et al., 2010). Overall most of the hypotheses for how Andean loading and
128 flexural subsidence initiated widespread deposition of the Solimões Formation are
129 generally qualitative in nature, and, as far as we are aware, no detailed flexural
130 calculations have yet been made to demonstrate such extensive subsidence. Given that
131 the Solimões Formation extends considerably far inland (as far east as the Purus Arch,
132 ~2000 km from the trench), affecting the pericratonic foreland, such as the Solimões
133 Basin (Fig. 1), additional explanations for such a broad episode of subsidence are
134 warranted. The concurrent relationship between basin development and drainage
135 reorganization with the arrival of the Peruvian flat-slab has been noted previously (e.g.
136 Latrubesse et al., 2010), but only isostatic or flexural influences associated with plate
137 interactions during flat-subduction were considered (i.e. rapid uplift of the Eastern

Cordillera and more extensive deformation in the Subandean foreland basins). This isostatic contribution to western Amazonian topography is estimated and discussed further in appendix A. The dynamic implications of the flat-slab arrival however and the resulting expression at the surface (i.e. the dynamic topography) is another potential source of topography that has yet to be considered.

Dynamic topography describes deflections of the Earth's surface that are supported dynamically by flow of the mantle below. In particular, convection of the mantle generates normal stresses that act at the base of the lithosphere, which deflects the lithosphere generating dynamic topography. For example a buoyant plume will rise, pushing up on the surface, producing dynamic uplift (e.g., Olson and Nam, 1986; Lithgow-Bertelloni and Silver, 1998). Likewise a dense slab will sink, pulling down on the surface, creating dynamic subsidence (e.g., Hager, 1984; Mitrovica et al., 1989). Such dynamic topography is not in isostatic equilibrium and has relatively low amplitude (~ 1 km) and long wavelength (typically 100's-1000's km) (Braun, 2010).

It has long been known that such deflections of the Earth's surface and its internal boundaries provide vital contributions to the long wavelength geoid (e.g. Hager et al., 1985). In the last decade or so the importance of dynamic topography at shorter wavelengths has also taken on increasing prominence, for example in the development of continental basins (Burgess et al., 1997; Heine et al., 2008), in Australia (Gurnis et al., 1998; Heine et al., 2010), in North America (Spasojevic et al., 2010; Liu and Nummedal, 2004; Liu et al., 2011; Jadamec et al., 2013) and in Africa (Pysklywec and Mitrovica, 1999). For South America there have been recent efforts to study dynamic topography of the continent as a whole (Shephard et al., 2010; Dávila and Lithgow-Bertelloni, 2013) as

well as focused investigation of the Argentine Pampas region (Dávila et al., 2010), and subduction of the Chile ridge beneath Patagonia (Guillaume et al., 2009). Shephard et al.'s (2010) study primarily focused on relating the drainage reorganization of Amazonia during the Miocene and the formation of the modern day Amazon River System, to the evolution of subduction driven dynamic topography. The geometry and density content of the subducted slabs beneath South America were derived from the global S-wave tomography of Grand (2002).

This type of approach however has two important caveats. Firstly, whilst first order changes in the Amazonian drainage are reproduced, the absolute amount of dynamic subsidence is too large. This is because the tomographic models provide a low-resolution image of a spatially large and high-density anomaly in the lower mantle. This expansive starting anomaly drives strong downwarping on the land above, predicting flooding over most of the South American continent. Evidence for flooding to this extent is not seen today nor in the geological record (Harrison et al., 1983; Hoorn, 2006; Lithgow-Bertelloni and Gurnis, 1997).

Secondly, variations in the subduction morphology and density content along strike are not reproduced. The western margin of South America is characterized by an alternating pattern of steep and flat slabs, but these are not easily observed by body-wave tomography, due to a lack of crossing ray-paths in the upper mantle. This is especially true for northern South America where station coverage is particularly poor. This is concerning because sensitivity kernels indicate that surface dynamic topography is particularly sensitive to upper mantle structure (whereas the geoid has a higher sensitivity to the lower mantle) (Hager and Richards, 1989). If we want to be able to match and

184 understand the geological history of a region (i.e. western Amazonia), then the details of
185 subduction in the upper mantle, such as along strike variations in slab dip and density
186 structure, are critical, not just to the tectonic component but also to the dynamic signal of
187 topography (Dávila et al., 2010, Dávila and Lithgow-Bertelloni, 2013).

188 Overall such broad view techniques tend to have difficulty replicating the local
189 geology at the surface, which closely depends on a broad range of factors. Namely the
190 interaction of both tectonic and dynamic controls on topography requires greater
191 consideration, as well as the along strike variability in subduction style. For western
192 Amazonia, a direct comparison of tectonics, flexural deformation, and dynamics of the
193 Peruvian flat-slab, with the subsurface sedimentary record has yet to be made. A
194 representation that takes such factors into account is therefore timely and required, so that
195 we can obtain a more complete picture of all the topographic forces that helped mold the
196 unique Amazon Basin.

197

198 **2. SLAB GEOMETRY AND DENSITY STRUCTURE**

199 The dynamic topography of flat-slab regions is currently a subject of debate. Flat-
200 slab episodes have often been equated with large shallow mass anomalies, resulting in
201 prominent long-wavelength dynamic subsidence and the formation of sedimentary basins
202 directly above them (e.g. Liu et al., 2011). Dávila et al. (2010) however demonstrated at
203 the modern Chilean/Argentine flat-slab segment that dynamic subsidence does not occur
204 directly over the flat slab but is instead offset to the east, where subduction steepens again
205 at the slab leading edge. Likewise for the Alaskan flat subduction zone, Jadamec et al.
206 (2013) suggest that the position of slab steepening is controlling the location of the Cook

207 Inlet Basin. Furthermore, Dávila and Lithgow-Bertelloni (2013) argue that flat-slab
208 segments should have neutral buoyancy based on evidence for abnormally thick oceanic
209 crust alongside a kinetically hindered basalt to eclogite reaction (e.g. Cembrano et al.,
210 2007; Gans et al., 2011). Several modeling studies demonstrate flattening of a slab when
211 over-thickened oceanic crust is subducted with partial to zero eclogitization (van Hunen,
212 2002a; 2002b; Arrial and Billen, 2013). Under this assumption flat-segments produce
213 little or no dynamic topography, meanwhile a shift from normal to flat-slab subduction
214 actually results in relative dynamic uplift over the transitioning region. This relationship
215 between flat-slabs and dynamic topography can therefore be constrained further by
216 studying present day, active systems such as in Peru and comparing the results with
217 geological observations.

218 Predictions of dynamic topography and their geological expression have been
219 shown to be highly sensitive to slab morphology and density structure i.e. the slab model
220 (Dávila et al., 2010; Jadamec et al., 2013). Previous predictions over the northern Andes
221 and western Amazonia region have used simplified models of the subducting slab. For
222 example, in global models, subduction zones are replicated by dropping slablets
223 vertically at the trench (e.g. Lithgow-Bertelloni and Gurnis, 1997). In regional models,
224 Dávila and Lithgow-Bertelloni (2013) took into account a more accurate flat-slab
225 morphology by modeling a horizontal segment under Peru and then a 30° dip further to
226 the east. Other models based on global S-wave tomography, such as Shephard et al.
227 (2010, 2012), typically struggle to resolve subducting slabs above the transition zone,
228 especially over South America where station coverage is lacking (Grand, 2002). Only
229 recently have seismic deployments been operating in Peru (e.g. PULSE and CAUGHT:

230 http://www.iris.edu/hq/science_highlights/pulse_and_caught_seismology_in_the_high_a
231 ndes, and PeruSE: http://www.gps.caltech.edu/~clay/PeruWeb/PeruSE.html), mostly
232 covering the southern portion of the flat-slab region. Tomographic resolution of the slab
233 will therefore likely improve in the future as new data and published results become
234 available. At the current time however, such a tomographic approach is unable to capture
235 the flat-slab shape of the downgoing Nazca plate, both in the most comprehensive global
236 studies (e.g. Li et al., 2008) and even from upcoming preliminary results of the regional
237 seismic projects (e.g. Scire et al., 2013).

238 Given the importance of the details of the slab model to the dynamic topography
239 predictions and therefore to connect with the geology, we aim to map out a realistic and
240 improved geometry of the Nazca slab. Based on the current available resources, this is
241 best achieved for the Peruvian flat-slab region by utilizing the seismicity (i.e. the Wadati-
242 Benioff Zone) to delineate the slab shape (Fig. 2a). Over 300 earthquakes (M > 3.0) from
243 the NEIC catalog were used (http://earthquake.usgs.gov/earthquakes/eqarchives/epic/).
244 This catalog contains events from 1970 to present and is the most complete and up-to-
245 date compilation available for the region. Events with depths shallower than 70
246 kilometers were removed to eliminate events that may have originated in the continental
247 lithosphere. Blockmean and surface gridding algorithms from GMT (Wessel and Smith,
248 1991) were then used to interpolate the points/events and recreate the inferred shape of
249 the slab down to 700 km. An extensive flat-slab segment is clearly reproduced (Fig. 2a
250 and 2c) by an abundance of seismicity in the 70-200 km depth plane, that extends ~500
251 km away from the trench. The slab model then rapidly drops off towards a cluster of deep
252 seismicity (500-700 km depth) further inland. Although there is a paucity of intermediate

253 seismicity, the leading edge of subduction in our model is well defined by the sharp
254 transition from shallow to deep events. It also matches well with preliminary
255 tomographic images of the Nazca slab in the upper mantle (with resolution below 200km)
256 using teleseismic body-waves (Scire et al., 2013).

257 Density anomalies (relative to background mantle, up to 50 kg/m^3) were also
258 assigned to the slab model based on the age of the subducting oceanic lithosphere at the
259 trench (Müller et al., 2008) (Fig. 2). For the segment where the slab is horizontal, the
260 density anomaly was set to zero ($\delta\rho$ = 0 kg/m^3) (analogous to the Pampean flat slab of
261 Dávila et al., 2010), to replicate neutral buoyancy. This assumption can be additionally
262 justified by initial surface-wave tomography results from the region (Knezevic
263 Antonijevic et al., 2013), based on data from the recent seismic deployments. These new
264 images show that the Peruvian flat-slab is predominantly low-velocity, indicating the
265 presence of lower density material relative to 'normal' subducted oceanic lithosphere (i.e.
266 dense sinking slabs), which typically display a high-velocity seismic signature. This
267 would suggest that the transition from basalt to higher density eclogite within the oceanic
268 crust is indeed undergoing a delay in the region of flat subduction.

269 In addition to a more realistic flat slab, we also made a slab model for normal
270 subduction, i.e. for a slab with uniform 30° dip angle (Fig. 2b and 2d), based on the
271 subduction angle to the north and south of the flat-slab region (Cahill and Isacks, 1992;
272 Phillips and Clayton, 2014). This is representative of how subduction may have looked
273 prior to the arrival of the flat slab. By comparing the two different slab models we are
274 able to visualize the temporal change in dynamic topography felt by the landscape since
275 the onset of slab flattening.

3. PREDICTED DYNAMIC TOPOGRAPHY AND FLEXURE

3.1.1 Dynamic Topography Computation and Results

We calculate the dynamic topography resulting from the instantaneous viscous flow induced by a prescribed density field (i.e. the slab), by solving the equations for the conservation of mass and momentum via propagator matrices in a spherical shell (Hager, 1984; Hager and O'Connell, 1979; 1981). Density and flow fields are computed to spherical harmonic degree and order 50 (plotted to degree 40). The mantle is assumed to have a Newtonian rheology and viscosity varies only with radius. The dynamic topography we calculate at any given time is independent of the absolute viscosity but the amplitude does depend on the relative viscosity contrast between each layer (the location of peak dynamic subsidence or uplift is unaffected). The rate of change of dynamic topography would however depend on the absolute viscosity. We present results for a viscosity structure of 10 for the lithosphere (which is uniformly 120 km thick) and 50 for the lower mantle as normalized to the upper mantle, based on the best correlation with the geoid (Ricard et al., 1993; Lithgow-Bertelloni and Richards, 1998) and consistent with previous studies (Lithgow-Bertelloni and Gurnis, 1997; Dávila et al., 2010). Using this mantle viscosity structure the dynamic topographies predicted by each of the slab models are shown in figure 2.

For the uniform 30° dip slab model, representing 'normal' subduction, dynamic subsidence is predicted underneath the Peru-Chile trench (thick black line in Fig. 2b). Taking into account a more realistic flat-slab model (Fig. 2a and 2c), dynamic subsidence is considerably offset from trench, by well over 1000 km inland. This depression is

299 located to the east of the flat-slab, directly over the region where the slab begins to
300 steepen again and sink back down into the mantle. In contrast, directly over the flat
301 segment, dynamic topography values are smaller (~500 m) and positive in value. For
302 both slab models the dynamic subsidence predicted is long-wavelength (~1500 km) and
303 comparatively high in amplitude (>1 km).

304 If we assume that our 'normal' slab model (uniform 30° dip) is representative of
305 subduction in the region prior to the arrival of the flat-slab (see also Dávila and Lithgow-
306 Bertelloni, 2013), then a transition from normal to flat subduction would predict transient
307 relative dynamic uplift across the Andes but relative dynamic subsidence within the distal
308 pericratonic foreland and western Amazonia (Fig. 3). Over time therefore we would
309 expect a wave of dynamic subsidence moving out from the trench, propagating eastwards
310 as the flat-slab develops, followed by a pulse of dynamic uplift behind it.

311

312 **3.1.2 Suitability of the Dynamic Topography Modeling Approach**

313 The dynamics of subduction systems are controlled by a competition between the
314 buoyancy forces (i.e. the slab model input), which drives the flow, and the rheology (i.e.
315 the viscosity profile), which acts to resist flow. When attempting to model these
316 dynamics there is usually a trade-off between capturing the complexity of the rheology
317 versus the buoyancy. To incorporate both realistic slabs (e.g. 3D geometries derived from
318 seismicity and lateral variations in slab buoyancy) as well as viscosity variations that can
319 cover many orders of magnitude (e.g. temperature and strain-rate dependence) requires
320 intensive computational power and time, on the order of several hundred processors for
321 days at a time for each model run (Jadamec et al., 2012; Jadamec et al., 2013), which can

322 be rather restrictive. For a comprehensive review of modeling mantle flow in subduction
323 zones see Billen (2008) and the references therein. In the case of our flow model, the
324 rheology is relatively simplified, including only radial variations in viscosity. By contrast,
325 we can easily include a high degree of detail in our slab morphology and buoyancy (on
326 the order of 0.5°x0.5°), whilst keeping the computational intensity low and accessible,
327 which allows one to sweep through many different morphological scenarios. Previous
328 similar studies have indicated that a high-resolution image of the slab, with density
329 structure varying over short length scales, is critical for correlating the dynamics with the
330 regional geology (Dávila et al., 2010; Dávila and Lithgow-Bertelloni, 2013; Jadamec et
331 al., 2013). Additionally recent observations of seismic anisotropy below the Peruvian
332 flat-slab strongly suggest that mantle flow in the region is closely tied to the local slab
333 morphology (Eakin and Long, 2013; Eakin et al., 2013). We therefore argue that as the
334 driver of flow, the buoyancy force is the main controlling process in subduction driven
335 dynamic topography.

336 If we were able to include rheological complexities in our flow models, then
337 lateral variations in viscosity would be the next step, most likely in the form of
338 temperature dependent viscosity. For example, cold subducting slabs are expected to
339 have a higher viscosity than the ambient mantle (King and Hager, 1994; Moresi and
340 Gurnis, 1996; Zhong and Davies, 1999), and as the viscosity of a slab increases, the
341 dynamic subsidence of the surface above also strengthens, deepening the dynamic basin
342 produced (Billen et al., 2003; Zhong and Gurnis, 1992; 1994; Moresi and Gurnis, 1996).
343 If this applied to the Peruvian subduction zone, then our estimate of dynamic subsidence
344 beneath western Amazonia, would represent a minimum (i.e. the true dynamic signal

345 could potentially be greater). The actual strength profile of subducting slabs is however
346 relatively uncertain and potentially rather complex (e.g. Hines and Billen, 2012). This
347 uncertainty increases even more for flat-slab regions such as Peru, where the slab
348 geometry and the material being subducted are atypical (i.e. the flat shape and subduction
349 of the Nazca Ridge), so we might not expect the same rheological properties to apply.

350 Even if we had a good idea of what the strength profile should be, the effect of
351 short wavelength viscosity variations on dynamic topography (and therefore the geoid) is
352 poorly understood (Billen et al., 2003) and difficult to constrain (Moucha et al., 2007). In
353 order to significantly impact our results, a large contrast in viscosity would most likely be
354 required. The most plausible way for this to occur would be via the presence of melt in
355 the mantle wedge to drastically lower the wedge viscosity. The wedge viscosity could
356 also be lowered by several orders of magnitude by the dislocation creep deformation
357 mechanism for olivine and the presence of high strain-rates i.e. such as expected in the
358 wedge (Jadamec and Billen, 2010; Stadler et al. 2010; Jadamec and Billen, 2012), though
359 the presence of melt would likely nullify this mechanism. Such a low viscosity wedge
360 (LVW) would act to decouple the slab from the surface, weaken the dynamic topography
361 and reduce the overall depth of the dynamic basin (Billen and Gurnis, 2001; Billen et al.,
362 2003). However this effect is limited, as dynamic topography is the result of normal
363 stresses, which will still be able to transmit through the asthenosphere to the surface even
364 when the asthenosphere is relatively weak (shear stresses however would be adversely
365 impacted). Additionally the potential impact of a LVW is restricted above the Peruvian
366 flat-slab where there is very little space available for mantle material between the flat-
367 slab and the overlying continental crust (Cahill and Isacks, 1992; Phillips and Clayton,

2014), but a LVW could exist to the east where the slab steepens and a thicker mantle wedge is present. However the entire region is void of contemporary arc-volcanism and so the fate of slab volatiles that would be required to initiate melt production and lower the wedge viscosity is very much unclear.

3.2 Estimation of Flexure

Dynamic topography is typically much broader and flatter than tectonically driven flexure. To demonstrate this, we also calculated flexure profiles for the region (Fig. 3 and Fig. 4), based on a balanced cross-section from Gotberg et al. (2010), which was the best and most detailed section available. This cross-section covers only the eastern part of the cordillera but models show that it is the loads which are the closest, up to 200 km from the basin, that have the most influence on the flexural subsidence (Garcia Castellanos et al., 2002). We therefore use the cross-section from Gotberg et al. (2010) to estimate the extent of crustal shortening and thus geometry of the Andean load that is adjacent to the foredeep. The flexure generated by this load depends on the lithosphere rigidity i.e. effective elastic thickness (Te) of the plate, in addition to other rheological parameters (e.g. Watts, 2001). We used two different Te estimates, 25 km and 40 km (cf. Pérez-Gussinyé et al., 2007; Tassara et al., 2007). These predict 2.8 to 3.6 km of sedimentary accommodation space next to the load but the flexural basin diminishes within about 100 km (gray shaded area in Fig. 4).

We show in appendix B that even if we consider a simpler cross-section across the full orogen (Fig. B.1), and vary the load distribution (Fig. B.2), the wavelength of the flexural basin remains on the order of 100 km (minimum: 69 km, maximum: 115 km).

391 Dávila and Lithgow-Bertelloni (2013) also show a similar result of <100 km width based
392 on cross-sections from Megard (1987) and Hermoza et al. (2005) that are less detailed
393 than what we use here. We expect therefore that the flexural subsidence should be an
394 order of magnitude narrower than the dynamic subsidence.
395
396 **4. IMPACT ON WESTERN AMAZONIA**
397 **4.1 Comparison with the Geological Record**
398 To constrain and interpret dynamic topography, we need to compare with
399 available geological proxies that are sensitive to topographic changes. Given that
400 sediment dynamics respond to gradient changes, not only in thicknesses but also in
401 facies, the stratigraphic record is a good proxy with which to compare our dynamic
402 topography predictions. We analyze the Solimões Formation that covers a large area of
403 western Amazonia (Fig. 1), extending from the most proximal foreland depocenters
404 (foredeep), to pericratonic settings (e.g. the Solimões Basin), located more than 500 km
405 away from the easternmost relief.
406 Given the inaccessibility and vastness of the Amazonia region, sampling of the
407 formation is difficult and sporadic, with most information sourced from riverbank
408 exposures and road cuts (Hoorn, 1993; 1994; Räsänen et al., 1995; Latrubesse et al.,
409 1997; 2007; 2010; Cozzuol, 2006; Wesselingh et al., 2006a; Gross et al., 2011; Rodrigues
410 Nogueira et al., 2013) or from wells drilled by hydrocarbon exploration in the 1970's
411 (Maia et al., 1977; Del'Arco et al., 1977; Hoorn, 1993; Wesselingh et al., 2006b; Silva-
412 Caminha et al., 2010; Wanderley-Filho et al., 2010). Based on these various geological
413 surveys an isopach map of the Solimões Formation is available (see Fig. 1 and Fig. 5c)

414 (Latrubesse et al., 2010), that illustrates the thicknesses of the sedimentary beds within
415 the Solimões and Acre basins (>1km in the Acre Basin). It should be noted that the
416 Solimões Formation is present over a much wider area (thick purple line in Fig. 1 and
417 Fig. 5c) than that covered by the availability of the isopachs, and that these isopachs
418 represent only the thickness of the Solimões Formation within the basins not the overall
419 basin depth (i.e. the Solimões Formation overlies older but less spatially extensive
420 Cretaceous and Paleozoic deposits that are not included).

421 As well as producing the isopach map the geological field studies indicate that the
422 Solimões unit consists mostly of fine-grained inter-bedded claystones, siltstones and
423 sandstones (Latrubesse et al., 2010; Rodrigues Nogueira et al., 2013). Interpretations of
424 the paleo-environmental history of this sedimentary record are widely varying and
425 extensively debated, ranging from marine influenced (Hoorn, 1993; 1994; Räsänen et al.,
426 1995; Roddaz et al., 1995), to mega-wetland or lacustrine dominated (Wesselingh et al.,
427 2002; Campbell et al., 2006; Hoorn et al., 2010a; 2010b), to fluvial dominated
428 (Latrubesse et al., 2007; 2010; Silva-Caminha et al., 2010; Gross et al., 2011; Rodrigues
429 Nogueira et al., 2013).

430 Given its large extent and widespread coverage the Solimões Formation is
431 therefore a good observational proxy with which to understand the subsidence history of
432 the region, and thus to compare with our dynamic topography and flexural models (Fig.
433 3). It is important to notice that this sedimentary accumulation extends beyond the zone
434 of flexural subsidence expected from the cordilleran loading (<300 km) and can not
435 therefore be easily explained by purely tectonic processes. The basin geometry,
436 specifically the location of the depocenter and maximum thickness (~1 km), does

however correlate remarkably well to the dynamic subsidence driven by the flat-slab morphology (Fig. 3 and Fig. 5c).

It is also important to emphasize that the development of the Peruvian flat slab and deposition of the Solimões Formation are contemporaneous, both having occurred from the Mid to Late Miocene and onwards (Hampel, 2002; Bissig et al., 2008; Ramos and Folguera, 2009; Hoorn, 1993; Wesselingh et al., 2006b; Latrubesse et al., 2010; Gross et al., 2011). In agreement with the flat subduction dynamics in Peru, there are also indications that the Solimões Formation gets younger towards the east. For example the formation is solely Upper Miocene in the Acre Basin to the west of the Iquitos Arch (Gross et al., 2011), but extends into the Pliocene in the Solimões Basin to the east of this arch (Silva-Caminha et al., 2010; Rodrigues Nogueira et al., 2013) (Fig. 5). Additionally it has been more precisely dated by Latrubesse et al. (2010) that the Solimões Formation only propagated east of the Iquitos Arch after 9-6 Ma. This eastward younging trend is consistent with our prediction that a wave of dynamic subsidence propagated out east from the Andes as slab flattening advanced in both space and time (Fig. 3). The difference in the age of the deposits across the Iquitos Arch, from older in the west to younger in the east, can therefore be easily explained by the transient dynamic signal from the formation of the flat-slab, with dynamic subsidence propagating eastward over time tracking the migration of the subduction leading edge.

4.2 Implications for the Evolution of Western Amazonia

Based on the above observations, we therefore propose that long wavelength dynamic topography associated with the transition from normal to flat-slab subduction

460 beneath Peru, as well as flexural subsidence in the proximal foreland basins, were both
461 important factors in the widespread subsidence and deposition of the Solimões Formation
462 across western Amazonia. Considering the interaction of both tectonic and dynamic
463 controls on topography, and with observations from the geological record, we
464 hypothesize the following model for the evolution of the Amazonian landscape, as
465 illustrated in Fig. 5.

466 Initially during the Early Miocene (Fig. 5a-b), before the Nazca Ridge arrived,
467 subduction was steeper beneath Peru compared to the present day. The Andes were
468 beginning to grow and the continent was deforming via crustal shortening and flexural
469 processes. At longer wavelengths there was also dynamic subsidence beneath the Andes
470 from mantle flow induced by the dipping slab. The flexural and dynamic basin would
471 have slowly filled with sediment, forming the first and oldest deposits of the Solimões
472 Formation (gray shaded region in Fig. 5b, and labeled as 1 in Fig. 5d). At this stage, the
473 Northern Cordillera was not fully established and drainage portals allowed access to the
474 Pacific Ocean and/or the Caribbean Sea (turquoise arrows in Fig. 5a).

475 Later as flat-slab subduction took hold during the Late Miocene (Fig. 5c-d), plate
476 coupling and tectonic deformation intensified along the northern Andes. Consequently
477 the northern Cordillera underwent a period of rapid growth, increasing the relief,
478 orogenic loading, erosional rates and sediment run-off, as well as triggering a further
479 deepening and broadening of the flexural basins, especially across the foredeep (Jordan
480 and Gardeweg, 1989; Kroonenberg et al., 1990; Hoorn et al., 1995; 2010; Nobret et al.,
481 1996; Garzione et al., 2008; Roddaz et al., 2010). Additional accommodation space for
482 the Solimões Formation was created from both this flexural subsidence driven by

483 orogenic deformation, as well as the propagation of longer wavelength dynamic
484 subsidence into the distal foreland. Whilst the tectonic signal has the primary control on
485 topography dominating where thick sedimentary sequences are preserved close to the
486 Andean Cordillera (i.e. several 1000's of kilometres thick within the foredeep)
487 (Wanderley-Filho et al., 2010), only the dynamic signal can explain the broad spatial
488 distribution of the Solimões Formation (Fig. 5c).

489 It has been proposed that as uplift progressed, an orogenic barrier was formed,
490 closing off the drainage pathways to the Pacific Ocean or Caribbean Sea (Hoorn et al.,
491 1995; 2010b; Hungerbühler et al., 2002; Campbell et al., 2006) and driving an eastward
492 sediment flux. Drainage pathways to the east however were partially blocked by the
493 Purus Arch (e.g. Figueiredo et al., 2009). Sediment eroded and transported from the
494 growing Andes was therefore carried to the western Amazonian lowlands and trapped in
495 continental basins that had been formed by flexural and dynamic subsidence (e.g. the
496 Acre and Solimões Basins) (Fig. 5c-d). These basins would have rapidly filled with the
497 large influx of sediment, transitioning from a possibly (mega-) wetland or lacustrine low-
498 energy low-circulation environment (similar to water filling up a bathtub), to more fluvial
499 domains as the basin became full, allowing for sediment to be transported by rivers
500 across the region rather then being trapped in the depression. Such a paleoenvironment
501 evolution is well represented by the depositional sequence of the Solimões Formation and
502 change in sedimentary facies from muddy (low energy conditions interpreted as
503 wetlands) to sandy (indicative of higher energy conditions, potentially fluvial) over time
504 (Hoorn et al., 2010b; Figueiredo 2012).

505 Once the basin became overfilled, drainage would have undergone reorganization
506 and it is possible that at this stage the eastern rim of the Solimões Basin was breached
507 (e.g. Campbell et al., 2006) connecting western Amazonia and the Andes to the Atlantic
508 Ocean, and thus establishing the transcontinental Amazon River like we see today (Fig.
509 5e). Large-scale deposition in western Amazonia would have ceased once sediment was
510 carried in vast quantities to the Atlantic Ocean. This is corroborated by an order of
511 magnitude increase in the mass accumulation rate of terrigeneous material on the
512 Amazon offshore fan beginning ~5 Ma (Dobson et al., 2001), at the same time that
513 deposition of the Solimões Formation in western Amazonia ceased (e.g. Latrubesse et al.,
514 2010), indicating that deposition of the bulk of Andean derived sediment switched from
515 the Amazonian lowlands to the Atlantic Ocean at this time.
516
517 **5. CONCLUSION**
518 Considering the Peruvian flat-slab morphology in detail predicts broad dynamic
519 subsidence that is significantly offset from the trench, by well over 1000 km inland. This
520 is in agreement with the geological record of deep sedimentary accumulations (up to 1
521 km thick) across western Amazonia, which lie too far from the orogenic front to be
522 explained by flexure alone. This has direct relevance for ancient episodes of flat-slab
523 subduction, such as the Cretaceous-Early Tertiary Laramide Orogeny, when dynamic
524 topography has been called upon to explain sedimentary basins and marine transgressions
525 within the western US interior (Liu et al., 2008; Mitrovica et al., 1989; Liu and
526 Nummedal, 2004). Modeling and observations across the Peruvian foreland reinforce the
527 notion (Dávila and Lithgow-Bertelloni, 2013; Jadamec et al., 2013) that slab flattening

produces subsidence far inland at the subduction leading edge, and that the transition from normal to flat subduction induces uplift over the flat-slab region itself.

Characterizing patterns of dynamic topography accurately is important if we want to understand how and why basins, as well as the overall landscape, have evolved over time. Our results and their agreement with the local geology imply that the influence of the 3D details of subduction on the dynamics, such as along strike variations in morphology, matter greatly to this goal. In the future, our ability to correctly predict dynamic topography will therefore improve with better knowledge of subduction zone structure. In particular better constraints on slab shape and density, potentially from seismic and gravitational studies, as well as more information on rheological properties, such as lateral variations in viscosity between the slab and the wedge, have the potential to refine the expression of flat-slab subduction on the Earth's surface both in the present and in the past.

ACKNOWLEDGEMENTS

The 7th Framework Program, Marie Curie Actions (ERC), supports our ANDyN project (Andes-Nazca Experiment) in the Andes. We also appreciated funds and support by SECyT-UNC, CONICET, and FONCyT from Argentina, Yale University, University College London, and NERC grant NE/J024813/1. We thank two anonymous reviewers for suggestions that greatly improved the manuscript.

REFERENCES

Aleman, A. M., 2006, The Peruvian flat-slab. Geological Society of America Abstracts with Programs, Speciality Meeting No. 2, p. 21.

552 Amante, C. and Eakins, B.W., 2009, ETOPO1 1 Arc-Minute Global Relief Model: Procedures, Data
553 Sources and Analysis. NOAA Technical Memorandum NESDIS NGDC-24, 19 pp, March 2009.
554 Arrial, P. A., and Billen, M. I., 2013, Influence of geometry and eclogitization on oceanic plateau
555 subduction. Earth and Planetary Science Letters, v. 363, p. 34-43.
556 Billen, M.I., 2008, Modeling the dynamics of subducting slabs. Annu. Rev. Earth Planet. Sci., v. 36, p. 325-
557 356.
558 Billen, M.I., and Gurnis, M., 2001, A low viscosity wedge in subduction zones. Earth Planet. Sci. Lett. v.
559 193, p. 227–36.
560 Billen, M.I., Gurnis, M., and Simons, M., 2003, Multiscale dynamic models of the Tonga- Kermadec
561 subduction zone. Geophys. J. Int. v. 153, p. 359–88.
562 Bird, P., 1988, Formation of the Rocky Mountains, western United States- a continuum computer model.
563 Science, v. 239, no. 4847, p. 1501–1507.
564 Bissig, T., Ullrich, T.D., Tosdal, R.M., Friedman, R., and Ebert, S., 2008, The time-space distribution of
565 Eocene to Miocene magmatism in the central Peruvian polymetallic province and its
566 metallogenetic implications. Journal of South American Earth Sciences, v. 26, p. 16-35.
567 Braun, J., 2010, The many surface expressions of mantle dynamics: Nature Geoscience, v. 3, no. 12, p.
568 825-833.
569 Burgess, P. M., Gurnis, M., and Moresi, L., 1997, Formation of sequences in the cratonic interior of North
570 America by interaction between mantle, eustatic, and stratigraphic processes. Geological Society
571 of America Bulletin, v. 109, no. 12, p. 1515-1535.
572 Cahill, T., and Isacks, B.L., 1992, Seismicity and Shape of the Subducted Nazca Plate. J. Geophys. Res., v.
573 97, no. B12, p. 17503-17529.
574 Campbell Jr., K.E., Frailey, C.D., and Romero Pitman, L., 2006. The Pan-Amazonian Ucayali peneplain,
575 Late Neogene sedimentation in Amazonia, and the birth of the modern Amazon River system.
576 Palaeogeography, Palaeoclimatology, Palaeoecology, v. 239, p. 166–219.
577 Capitanio, F.A., and Faccenda, M., 2012, Complex mantle flow around heterogeneous subducting oceanic
578 plates. Earth and Planetary Science Letters, v. 353, p. 29-37.
579 Cembrano, J., Lavenu, A., Yañez, G., Riquelme, R., Garcia, M., González, and G., Herail, G., 2007,

580 Neotectonics. In: Moreno, T., Gibbons, W. (Eds.), The Geology of Chile, The Geological Society,
581 London, p. 147-178.
582 Cozzuol, M., 2006. The Acre vertebrate fauna: diversity, geography and time. Journal of South American
583 Earth Sciences, v. 21, p. 185–203.
584 Dávila, F.M., Lithgow-Bertelloni, C., and Giménez, M., 2010, Tectonic and dynamic controls on the
585 topography and subsidence of the Argentine Pampas: The role of the flat slab. Earth Planet. Sci.
586 Lett., v. 295, no. 1, p. 187-194.
587 Dávila, F.M., and Lithgow-Bertelloni, C., 2013, Dynamic topography in South America. Journal of South
588 American Earth Sciences, v. 43, p. 127-144.
589 Del' Arco, J.O., Santos, R.O.B., Rivetti, M., Olivera Alves, E.D., Fernandes, C.A.C., Silva, L.L., 1977.
590 Folha SB. 19 Juruá. IeGeologia. Projeto Radambrasil. Levantamento de Recursos Naturais, v. 15,
591 p. 19-88.
592 Dickinson, W., and Snyder, W., 1978, Plate tectonics of the Laramide orogeny. Geol. Soc. Am. Mem., v.
593 151, p. 355–366.
594 Dobson, D.M., Dickens, G.R., and Rea, D.K., 2001, Terrigenous sediment on Ceara Rise: a Cenozoic
595 record of South American orogeny and erosion. Palaeogeography, Palaeoclimatology,
596 Palaeoecology, v. 165, p. 215–229.
597 Eakin, C. M., and Long, M. D., 2013. Complex anisotropy beneath the Peruvian flat slab from frequency-
598 dependent, multiple-phase shear wave splitting analysis. Journal of Geophysical Research: Solid
599 Earth, v. 118, doi:10.1002/jgrb50349.
600 Eakin, C. M., Long, M. D., Beck, S.L., Wagner, L.S., and Tavera, H., 2013, Characterizing Seismic
601 Anisotropy across the Peruvian Flat-Slab Subduction Zone: Shear Wave Splitting from PULSE,
602 AGU Fall Meeting 2013, San Francisco, CA.
603 Espurt, N., Funiciello, F., Martinod, J., Guillaume, B., Regard, V., Faccenna, C., and Brusset, S., 2008, Flat
604 subduction dynamics and deformation of the South American plate: Insights from analog
605 modeling. Tectonics, v. 27, TC3011, doi:10.1029/2007TC002175.
606 Figueiredo, J.J.P., 2012. Comment by JP Figueiredo, and Hoorn, C. on 'Late Miocene sedimentary
607 environments in south-western Amazonia (Solimoes Formation; Brazil)' by Martin Gross, Werner

E. Piller, Maria Ines Ramos, Jackson Douglas da Silva Paz. Journal of South American Earth Sciences, v. 35, p. 74–75.

Figueiredo, J., Hoorn, C., van der Ven, P. and Soares, E., 2009, Late Miocene onset of the Amazon River and the Amazon deep-sea fan: Evidence from the Foz do Amazonas Basin: Geology, v. 37, no. 7, p. 619–622.

Gans, C., Beck, S., Zandt, G., Gilbert, H., and Alvarado, P., 2011, Continental and oceanic crustal structure of the Pampean at slab region, western Argentina, using receiver function analysis: new high-resolution results: Geophysical Journal International, v. 186, p. 45-58.

Garcia-Castellanos, D., Fernandez, M., and Torné, M., 2002, Modeling the evolution of the Guadalquivir foreland basin (southern Spain). Tectonics, v. 21, no. 3, doi:10.1029/2001TC001339.

Garzione, C.M., Molnar, P., Libarkin, J.C., and Mc Fadden, B.J., 2007. Rapid late Miocene rise of the Bolivian Altiplano: evidence for removal of mantle lithosphere. Earth and Planet Science Letter, v. 241, p. 543–556.

Gotberg, N., McQuarrie, N., and Carlotto Caillaux, V., 2010, Comparison of crustal thickening budget and shortening estimates in southern Peru (12 −14°S): Implications for mass balance and rotations in the "Bolivian orocline". Geological Society of America Bulletin, v. 122, no. 5-6, p. 727-742, doi: 10.1130/B26477.1.

Grand, S. P., 2002, Mantle shear wave tomography and the fate of subducted slabs. Phil. Trans. R. Soc. Lond. A, v. 360, p. 2475–2491.

Gripp, A.E. and Gordon, R.G., 2002, Young tracks of hotspots and current plate velocities. Geophys. J. Int., v. 150, no. 2, p. 321–361.

Gross, M., Piller, W.E., Ramos, M.I., and da Silva Paz, J.D., 2011, Late Miocene sedimentary environments in south-western Amazonia (Solimões Formation; Brazil). Journal of South American Earth Sciences, v. 32, p. 169–181.

Guillaume, B., Martinod, J., Husson, L., Roddaz, M., and Riquelme, R., 2009, Neogene uplift of central eastern Patagonia: Dynamic response to active spreading ridge subduction?. Tectonics, v. 28, TC2009, doi:10.1029/2008TC002324.

635 Gurnis, M., Müller, R. D., and Moresi, L., 1998, Cretaceous vertical motion of Australia and the Australian
636 Antarctic discordance. Science, v. 279, p. 1499-1504.
637 Gutscher, M.A., Maury, R., Eissen, J.P., and Bourdon, E., 2000a, Can slab melting be caused by flat
638 subduction. Geology, v. 28, p. 535–538.
639 Gutscher, M.A., Spakman, W., Bijwaard, H., and Engdahl, E. R., 2000b, Geodynamics of flat subduction:
640 Seismicity and tomographic constraints from the Andean margin, Tectonics, v. 19, no. 5, p. 814–
641 833.
642 Hager, B.H., 1984, Subducted Slabs and the Geoid: Constraints on Mantle Rheology and Flow. J. Geophys.
643 Res., v. 89, no. B7, p. 6003–6015.
644 Hager, B.H., Clayton, R.W., Richards, M.A., Comer, R.P., and Dziewonski, A.M., 1985, Lower mantle
645 heterogeneity, dynamic topography and the geoid. Nature, v. 313, p. 541-545.
646 Hager, B. H., and O'Connell, R. J., 1979, Kinematic models of large-scale flow in the Earth's
647 mantle. Journal of Geophysical Research: Solid Earth, v. 84, no. B3, p. 1031-1048.
648 Hager, B.H., and O'Connell, R.J., 1981, A simple global model of plate dynamics and mantle
649 convection. Journal of Geophysical Research: Solid Earth, v. 8, no. B6, p. 4843-4867.
650 Hager, B.H., and Richards, M.A., 1989, Long-wavelength variations in Earth's geoid: Physical models and
651 dynamical implications. Philosophical Transactions of the Royal Society of London. Series A,
652 Mathematical and Physical Sciences, v. 328, no. 1599, p. 309-327.
653 Hampel, A., 2002. The migration history of the Nazca Ridge along the Peruvian active margin: a re-
654 evaluation. Earth and Planetary Science Letters, v. 203, p. 665– 679.
655 Harrison, C. G. A., Miskell, K. J., Brass, G. W., Saltzman, E. S., and Sloan, J. L., 1983, Continental
656 hypsography. Tectonics, v. 2, no. 4, p. 357-377.
657 Heine, C., Müller, R. D., Steinberger, B., and DiCaprio, L., 2010. Integrating deep Earth dynamics in
658 paleogeographic reconstructions of Australia. Tectonophysics, v. 483, no. 1, p. 135-150.
659 Heine, C., Muller, R., Steinberger, B. and Torsvik, T., 2008, Subsidence in intracontinental basins due to
660 dynamic topography. Phys. Earth Planet. Inter., v. 171, p. 252–264.
661 Henry, S.G., and Pollack, H.N., 1988, Terrestrial heat flow above the Andean subduction zone in Bolivia
662 and Peru. Journal of Geophysical Research, v. 93, no. B12, p. 15153-15162.

663 Hermoza, W., Brusset, S., Baby, P., Gil, W., Roddaz, M., Guerrero, N., and Bolaños, R., 2005, The
664 Huallaga foreland basin evolution: Thrust propagation in a deltaic environment, northern Peruvian
665 Andes. Journal of South American Earth Sciences, v. 19, no. 1, p. 21-34.
666 Hines, J. M., and Billen, M. I., 2012, Sensitivity of the short-to intermediate-wavelength geoid to rheologic
667 structure in subduction zones. Journal of Geophysical Research: Solid Earth, v. 117, B05410,
668 doi:10.1029/2011JB008978.
669 Hoorn, C., 1993, Marine incursions and the influence of Andean tectonics on the Miocene depositional
670 history of northwestern Amazonia: results of a palynostratigraphic study. Palaeogeogr.,
671 Palaeoclimatol., Palaeoecol., v. 105, p. 267–309.
672 Hoorn, C., 1994, An environmental reconstruction of the palaeo-Amazon River system (Middle-Late
673 Miocene, NW Amazonia). Palaeogeography, Palaeoclimatology, Palaeoecology, v. 112, no. 3, p.
674 187-238.
675 Hoorn, C., 2006, The birth of the mighty Amazon. Scientific American, v. 294, no. 5, p. 52-59.
676 Hoorn, C., Guerrero, J., Sarmiento, G.A., and Lorente, M.A., 1995, Andean tectonics as a cause for
677 changing drainage patterns in Miocene northern South America. Geology, v. 23, no. 3, p. 237-240.
678 Hoorn, C., Wesselingh, F.P., Ter Steege, H., Bermudez, M.A., Mora, A., Sevink, J., and Antonelli, A.,
679 2010a, Amazonia through time: Andean uplift, climate change, landscape evolution, and
680 biodiversity. Science, v. 330, no. 6006, p. 927-931.
681 Hoorn, C., Wesselingh, F. P., Hovikoski, J., and Guerrero, J. 2010b. The Development of the Amazonian
682 Mega-Wetland (Miocene; Brazil, Colombia, Peru, Bolivia). In: C. Hoorn, F.P. Wesselingh (Eds.),
683 Amazonia, landscape and species evolution: a look into the past, Wiley-Blackwell, Chichester, p.
684 123-142.
685 Hungerbühler, D., Steinmann, J., Winkler, W., Seward, D., Egüez, A., Peterson, D.E., Helg, U., and
686 Hammer, C., 2002. Neogene stratigraphy and Andean geodynamics of southern Ecuador. Earth-
687 Science Reviews, v. 57, p. 75–124.
688 Jadamec, M. A., and Billen, M. I., 2010, Reconciling surface plate motions with rapid three- dimensional
689 mantle flow around a slab edge. Nature, v. 465, no. 7296, p. 338-341.
690 Jadamec, M. A., and Billen, M. I., 2012, The role of rheology and slab shape on rapid mantle flow: Three-

dimensional numerical models of the Alaska slab edge. Journal of Geophysical Research: Solid Earth, v. 117, B02304, doi:10.1029/2011JB008563.

Jadamec, M. A. , Billen, M. I., and Kreylos, O., 2012, Three-dimensional simulations of geometrically complex subduction with large viscosity variations. *ACM Proceedings of the 2012 Conference on eXtreme Science and Engineering Discovery Environment*.

Jadamec, M. A., Billen, M. I., and Roeske, S. M., 2013, Three-dimensional numerical models of flat slab subduction and the Denali fault driving deformation in south-central Alaska. Earth and Planetary Science Letters, v. 376, p. 29-42.

Jordan, T.E., and Gardeweg, P.M., 1989, Tectonic evolution of the late Cenozoic central Andes (20°–33°S). In: Ben-Avraham, Z. (Ed.), The Evolution of the Pacific Ocean Margins. Oxford University Press, New York, p. 193–207.

King, S. D., and B. H. Hager, 1994, Subducted slabs and the geoid: 1. Numerical experiments with temperature-dependent viscosity, J. Geophys. Res., v. 99, no. B10, p. 19843–19852.

Knezevic Antonijevic, S., Wagner, L.S., Beck, S.L., Zandt, G., and Long, M.D., 2013, Exposing the Peruvian Flat Slab from Shear Wave Velocity Structure, AGU Fall Meeting 2013, San Francisco, CA.

Kroonenberg, S.B., Bakker, J.G.M., and van der Weil, A.M., 1990. Late Cenozoic uplift and paleogeography of the Colombian Andes: constraints in the development of high-Andean biota. Geologie en Mijnbouw, v. 69, p. 279–290.

Latrubesse, E.M., Bocquentin, J., Santos, C.R., and Ramonell, C.G., 1997, Paleoenvironmental model for the late Cenozoic southwestern Amazonia paleontology and geology. Acta Amazonica, v. 27, p.103–118.

Latrubesse, E., Silva, S.F., Cozzuol, M., and Absy, M.L., 2007, Late Miocene continental sedimentation in the southwestern Amazonia and its regional significance: Biotic and geological evidence. Journal of South American Earth Science, v. 23, p. 61–80.

Latrubesse, E.M., Cozzuol, M., da Silva-Caminha, S.A.F., Rigsby, C.A., Absy, M.L., and Jaramillo, C., 2010, The Late Miocene paleogeography of the Amazon Basin and the evolution of the Amazon River system: Earth-Science Reviews, v. 99, no. 3, p. 99-124.

719 Li, C., van der Hilst, R.D., Engdahl, E.R., and Burdick, S., 2008, A new global model for P wave speed
720 variations in Earth's mantle. Geochemistry, Geophysics, Geosystems, v. 9, no. 5.
721 Lithgow-Bertelloni, C., and Gurnis, M., 1997, Cenozoic subsidence and uplift of continents from time-
722 varying dynamic topography. Geology, v. 25, no. 8, p. 735-738.
723 Lithgow‐Bertelloni, C., and Richards, M. A., 1998, The dynamics of Cenozoic and Mesozoic plate
724 motions. Reviews of Geophysics, v. 36, no. 1, p. 27-78.
725 Lithgow-Bertelloni, C., and Silver, P. G., 1998, Dynamic topography, plate driving forces and the African
726 superswell. Nature, v. 395, p. 269-272.
727 Liu, S., and Nummedal, D., 2004, Late Cretaceous subsidence in Wyoming: quantifying the dynamic
728 component. Geology, v. 32, no. 5, p. 397–400.
729 Liu, L., Spasojević, S., and Gurnis, M., 2008, Reconstructing Farallon plate subduction beneath North
730 America back to the Late Cretaceous. Science, v. 322, no. 5903, p. 934-938.
731 Liu, S., Nummedal, D., and Liu, L., 2011, Migration of dynamic subsidence across the Late Cretaceous
732 United States Western Interior Basin in response to Farallon plate subduction. Geology, v. 39, no.
733 6, p. 555 - 558.
734 Lonsdale, P., 2005, Creation of the Cocos and Nazca plates by fission of the Farallon plate.
735 Tectonophysics, v. 404, no. 3-4, p. 237-264.
736 Maia, R.G., Godoy, H.K., Yamaguti, H.S., Moura, P.D., Costa, F.D., Holanda, M.D., and Costa, J., 1977,
737 Costa Projeto de Carvao no Alto Solimões. Relatorio Final, Companhia de Pesquisa de Recursos
738 Minerais-Departamento Nacional da Produçáo Mineral, Manaus, p. 137.
739 Martinod, J., Husson, L., Roperch, P., Guillaume, B., and Espurt, N., 2010, Horizontal subduction zones,
740 convergence velocity and the building of the Andes. Earth and Planetary Science Letters, v. 299,
741 no. 3, p. 299-309.
742 Mégard, F., 1987, Cordilleran Andes and Marginal Andes: a review of Andean geology north of the Arica
743 Elbow (18°S). In: J.W.H. Monger, J. Francheteau (Eds.), Circum-pacific Orogenic Belts and
744 Evolution of the Pacific Ocean Basin. American Geophysical Union, Geological Society of
745 America, Geodynamic Series, vol. 18 (1987), pp. 71–95.

746 Mitrovica, J.X., Beaumont, C., and Jarvis, G.T., 1989, Tilting of the continental interior by the dynamical
747 effects of subduction. Tectonics, v. 8, no. 5, p. 1079–1094.
748 Mora, A., Baby, P., Roddaz, M., Parra, M., Brusset, S., Hermoza, W., and Espurt, N., 2010, Tectonic
749 History of the Andes and Sub–Andean Zones: Implications for the Development of the Amazon
750 Drainage Basin. In: C. Hoorn, F.P. Wesselingh (Eds.), Amazonia, landscape and species
751 evolution: a look into the past, Wiley-Blackwell, Chichester, p. 38-60.
752 Moresi, L., and Gurnis, M., 1996. Constraints on the lateral strength of slabs from three- dimensional
753 dynamic flow models. Earth Planet. Sci. Lett. v. 138, p. 15–28.
754 Moucha, R., Forte, A., Mitrovica, J., and Daradich, A., 2007, Lateral variations in mantle rheology:
755 Implications for convection related surface observables and inferred viscosity models. Geophys. J.
756 Int., v. 169, p. 113–135, doi:10.1111/ j.1365-246X.2006.03225.x.
757 Müller, R.D., Sdrolias, M., Gaina, C., and Roest, W.R., 2008, Age, spreading rates, and spreading
758 asymmetry of the world's ocean crust. Geochemistry Geophysics Geosystems, v. 9, no. 4, p. 18-
759 36.
760 Nobret, V., Lavenu, A., and Marocco, R., 1996, Concept of continuum as opposed to periodic tectonism in
761 the Andes. Tectonophysics, v.255, p. 65–78.
762 Olson, P., and Nam, S., 1986, Formation of seafloor swells by mantle plumes. J. Geophys. Res., v. 91, no.
763 B7, p. 7181–7191.
764 Pérez-Gussinyé, M., Lowry, A.R., and Watts, A.B., 2007, Effective elastic thickness of South America and
765 its implications for intracontinental deformation. Geochem. Geophys. Geosys., v. 8, no. 5, p. 1-22,
766 doi:10.1029/2006GC001511.
767 Phillips, K., and Clayton, R.W., 2014, Structure of the subduction transition region from seismic array data
768 in southern Peru, Geophysical Journal International, ggt504.
769 Pilger, R.H., 1981, Plate reconstructions, aseismic ridges, and low-angle subduction beneath the Andes.
770 Geological Society of America Bulletin, v. 92, p. 338–456.
771 Potter, P.E., 1997, The mesozoic and cenozoic drainage of South America: a natural history. Journal of
772 South American Earth Sciences, v. 10, p. 331–344.
773 Pysklywec, R. and Mitrovica, J., 1999, The role of subduction-induced subsidence in the evolution of the

774 Karoo Basin., J. Geol., v. 107, p. 155–164.
775 Ramos, V.A. and Folguera, A., 2009, Andean flat-slab subduction through time. From: Murphy, J. B.,
776 Keppie, J. D.and Hynes, A. J. (eds) Ancient Orogens and Modern Analogues. Geological Society
777 London Special Publication, v. 327, p. 31–54.
778 Räsänen, M., Linna, A.M., Santos, J.C.R., and Negri, F.R., 1995, Late Miocene tidal deposits in the
779 Amazonian foreland basin. Science, v. 269, p. 386–389.
780 Ricard, Y., Richards, M., Lithgow-Bertelloni, C., and LeStunff, Y., 1993, A geodynamical model of mantle
781 density heterogeneity. J. Geophys. Res., v. 98, no. B12, p. 21895–21909.
782 Roddaz, M., Viers, J., Brusset, S., Baby, P., and Hérail, G., 2005, Sediment provenances and drainage
783 evolution of the Neogene Amazonian foreland basin. Earth and Planetary Science Letters, v. 239,
784 no. 1, p. 57-78.
785 Roddaz, M., Hermoza, W., Mora, A., Baby, P., Parra, M., Christophoul, F., and Espurt, N., 2010, Cenozoic
786 sedimentary evolution of the Amazonian foreland basin system. In: C. Hoorn, F.P. Wesselingh
787 (Eds.), Amazonia, landscape and species evolution: a look into the past, Wiley-Blackwell,
788 Chichester, p. 61-88.
789 Rodrigues Nogueira, A. C., Silveira, R., and Felix Guimarães, J. T., 2013, Neogene-Quaternary
790 sedimentary and paleovegetation history of the eastern Solimões Basin, central Amazon region.
791 Journal of South American Earth Sciences, v. 46, p. 89-99.
792 Rosenbaum, G., Giles, D., Saxon, M., Betts, P.G., Weinberg, R.F., Duboz, C., 2005. Subduction of the
793 Nazca Ridge and the Inca Plateau: insights into the formation of ore deposits in Peru. Earth and
794 Planetary Science Letters, v. 239, p. 18–32.
795 Scire, A.C., Biryol, C.B., Zandt, G., Beck, S.L., Wagner, L.S., Long, M.D., Minaya, E., and Tavera, H.,
796 2013, Tomographic imaging of the Nazca slab and surrounding mantle in the mantle transition
797 zone beneath the Central Andes, AGU Fall Meeting 2013, San Francisco, CA.
798 Shephard, G.E., Müller, R.D., Liu, L., and Gurnis, M., 2010, Miocene drainage reversal of the Amazon
799 River driven by plate–mantle interaction. Nature Geoscience, v. 3, no. 12, p. 870-875.
800 Shephard, G.E., Liu, L., Müller, R.D., and Gurnis, M., 2012, Dynamic topography and anomalously
801 negative residual depth of the Argentine Basin. Gondwana Research, v. 22, no. 2, p. 658-663.

802 Siebert, L. and Simkin, T., 2002-, Volcanoes of the World: an Illustrated Catalog of Holocene Volcanoes
803 and their Eruptions: Smithsonian Institution, Global Volcanism Program Digital Information
804 Series, GVP-3, (http://www.volcano.si.edu/world/).
805 Silva-Caminha, S.A.F., Jaramillo, C., Absy, M.L., 2010, Neogene palynology of the Solimões Basin,
806 Brazilian Amazonia. Palaeontographica, v. 283, no. 1-3, p. 1–67.
807 Spasojevic, S., Liu, L. and Gurnis, M., 2009. Adjoint models of mantle convection with seismic, plate
808 motion, and stratigraphic constraints: North America since the Late Cretaceous. Geochem.
809 Geophys. Geosyst., v. 10, Q05W02.
810 Soler, P., and Bonhomme, M., 1990, Relations of Magmatic Activity to Plate Dynamics in Central Peru
811 from Late Cretaceous to Present. In: Kay, S., Rapela, C. (Eds.), Plutonism from Antarctica to
812 Alaska, Geol. Soc. Am. Mem., pp. 173–191.
813 Stadler, G., Gurnis, M., Burstedde, C., Wilcox, L. C., Alisic, L., and Ghattas, O., 2010, The dynamics of
814 plate tectonics and mantle flow: From local to global scales. Science, v. 329, no. 5995, p. 1033-
815 1038.
816 Tassara, A., Swain, C., Hackney, R., and Kirby, J., 2007, Elastic thickness structure of South America
817 estimated using wavelets and satellite-derived gravity data. Earth Planet. Sci. Lett., v. 253, no. 1,
818 p. 17-36.
819 van Hunen, J., van den Berg, A. P., and Vlaar, N. J., 2002a, On the role of subducting oceanic plateaus in
820 the development of shallow flat subduction. Tectonophysics, v. 352, p. 317 – 333,
821 doi:10.1016/S00401951(02)00263-9.
822 van Hunen, J., van den Berg, A. P., and Vlaar, N. J., 2002b, The impact of the South American plate
823 motion and the Nazca Ridge subduction on the flat subduction below South Peru. Geophys. Res.
824 Lett., v. 29, no. 14, doi:10.1029/2001GL014004.
825 Wanderley-Filho, J.R., and J.B.S. Costa, 1991, Contribuição à evolução estrutural de bacia do Amazonas e
826 sua relação com o embasamento. In: Simpósio de Geologica de Amazônia, 3, Anais. Belém:
827 Sociedade Brasileira de Geologia, pp. 244-259.
828 Wanderley-Filho, J.R., Eiras, J.F., Cunha, P.R.C., and P.H. Van der Vem, 2010, The Paleozoic Solimões
829 and Amazonas basins and the Acre foreland basin of Brazil. In: C. Hoorn, F.P. Wesselingh (Eds.),

Amazonia, landscape and species evolution: a look into the past, Wiley-Blackwell, Chichester, p. 9–28.

Watts, A. B., 2001, Isostasy and Flexure of the Lithosphere. Cambridge University Press, Cambridge.

Wessel, P., and Smith, W.H.F., 1991, Free software helps map and display data. Eos, Transactions American Geophysical Union, v. 72, no. 41, p. 441-446.

Wesselingh, F.P., Räsänen, M.E., Irion, G., Vonhof, H.B., Kaandorp, R., Renema, W., Romero Pittman, L., and Gingras, M., 2002, Lake Pebas: a palaeoecological reconstruction of a Miocene, long-lived lake complex in western Amazonia. Cainozoic Research, v. 1, p. 35–81.

Wesselingh, F.P., Ranzy, A., and Rasanen, M., 2006a, Miocene freshwater Mollusca from western Brazilian Amazonia. Scripta Geologica, v. 133, p. 419–437.

Wesselingh, F.P., Guerrero, J., Räsänen, M., Romero Pitmann, L. and H. Vonhof, 2006b, Landscape evolution and depositional processes in the Miocene Amazonian Pebas lake/wetland system: evidence from exploratory boreholes in northeastern Peru. Scripta Geologica, v. 133, p. 323-361.

Zhong S, and Davies G.F., 1999, Effects of plate and slab viscosities on the geoid. Earth Planet. Sci. Lett., v. 170, p. 487–496.

Zhong S, and Gurnis M. 1992. Viscous flow model of a subduction zone with a faulted lithosphere: long and short wavelength topography, gravity and geoid. Geophys. Res. Lett., v.19, no. 18, p. 1891–94.

Zhong S, and Gurnis M. 1994. Controls on trench topography from dynamic models of subducted slabs. J. Geophys. Res., v. 99, no. B8, p. 15683–95.

FIGURES

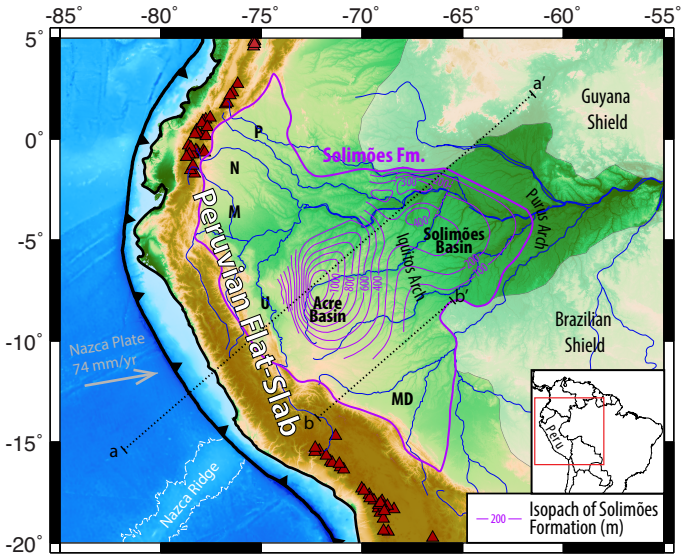

Figure 1. Tectonic setting of Peruvian flat-slab subduction and western Amazonia. The inset map highlights the study location and political boundaries for context. The total area thought to be covered by the Solimões Formation is outlined by the thick purple line, based on the maps of Hoorn (1994). This includes many different individual basins such as the Acre and the Solimões, as well as other foreland basins represented by the letters (P: Putumayo, N: Napo, M: Marañon, U: Ucayali, MD: Madre de Dios). Isopachs of the Solimões Formation thickness in the Acre and Solimões Basins are available and shown in purple after Latrubesse et al., (2010). Volcano locations (red triangles) are from Siebert and Simkin (2002). The gray arrow represents the absolute plate motion of the Nazca plate from HS3-NUVEL1A (Gripp and Gordon, 2002). The dotted black lines represent locations of cross-sections in Fig. 3 (a-a') and location of the flexural calculation in Fig. 4 (b-b').

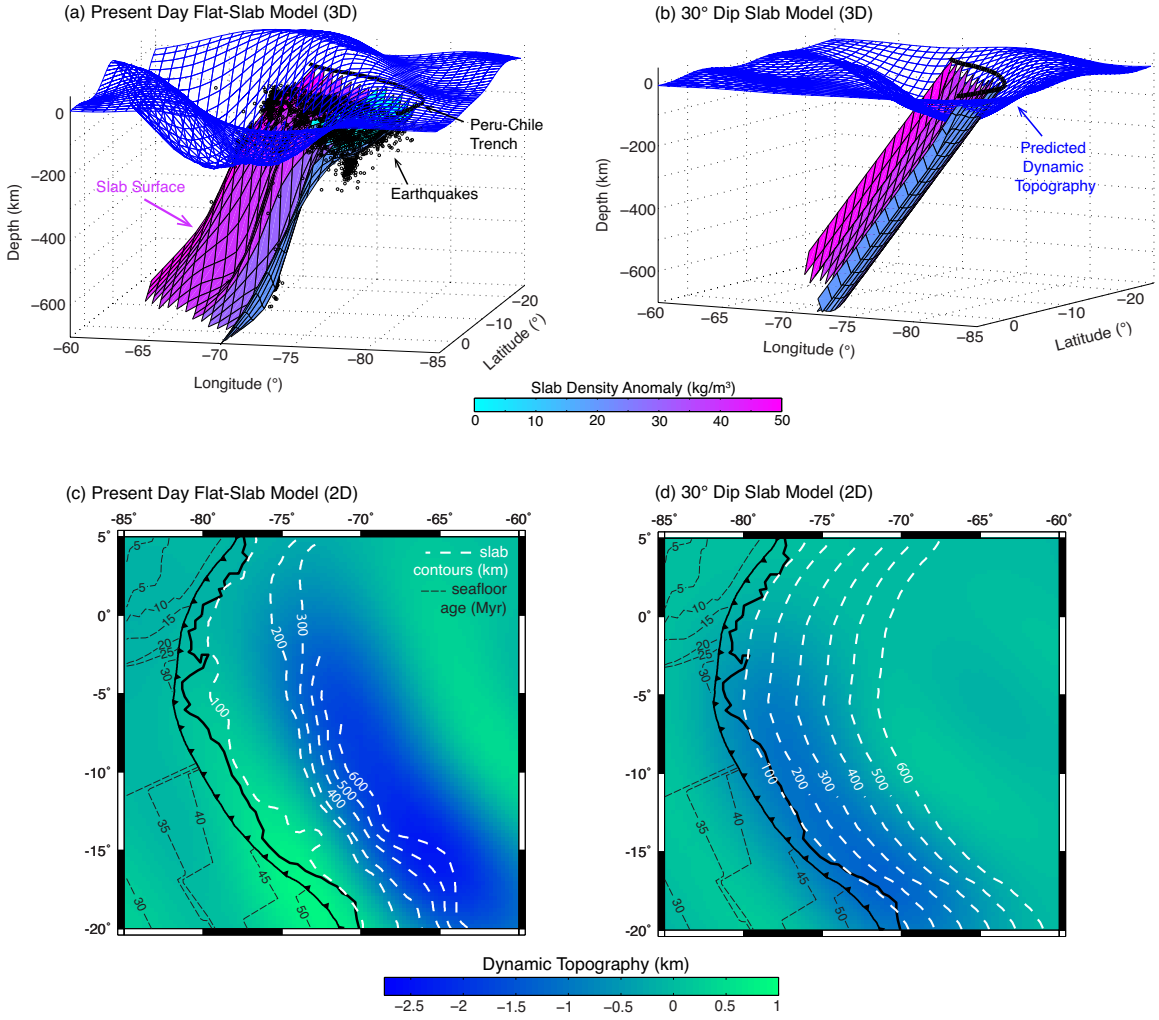

Figure 2. Comparison of dynamic topography predicted by two different slab models for the Peruvian subduction zone, shown in 3D (top row) and 2D (bottom row). The left hand side (a and c) represents the present day 3D flat-slab morphology determined from local seismicity (small black circles give individual earthquake locations), whilst the right hand side (b and d) reflects the uniform 30° dip slab model akin to 'normal' subduction before the onset of slab flattening. (a-b) Dynamic topography (blue mesh surfaces) has been vertically exaggerated for illustrative purposes and plotted up to spherical harmonic degree 40. The slab surfaces are colour-coded according to the density anomaly assigned.

(c-d) Same as figures (a-b) but now in map view, comparing the dynamic topography against the slab contours (white dashed lines). Contours of seafloor age (on which the density anomalies are based) are from Müller et al. (2008).

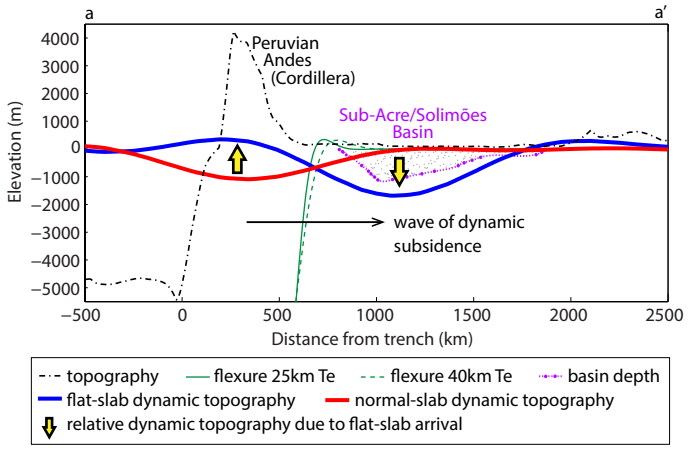

Figure 3. Profiles illustrating the different contributions on the total topography across the Amazonian foreland. The thick profiles depict the impact of relative dynamic topography given a transition from 'normal' subduction (thick red line) to flat-slab subduction (thick blue line) (see location of the profile a-a' in Fig. 1). This results in relative dynamic uplift beneath the Peruvian Andes (High Cordillera) but relative dynamic subsidence beneath the western Amazon Basin (distal foreland). The Sub-Acre/Solimões basin (gray dotted region) is outside the influence of flexure driven by the mountain loading (thin green lines), but does coincide with relative dynamic subsidence from the arrival of the flat-slab. Depth of the basin (dotted purple line) determined from an isopach map (Latrubesse et al., 2010). Present-day topography (dot-dash black line) taken from ETOPO1 (Amante and Eakins, 2009).

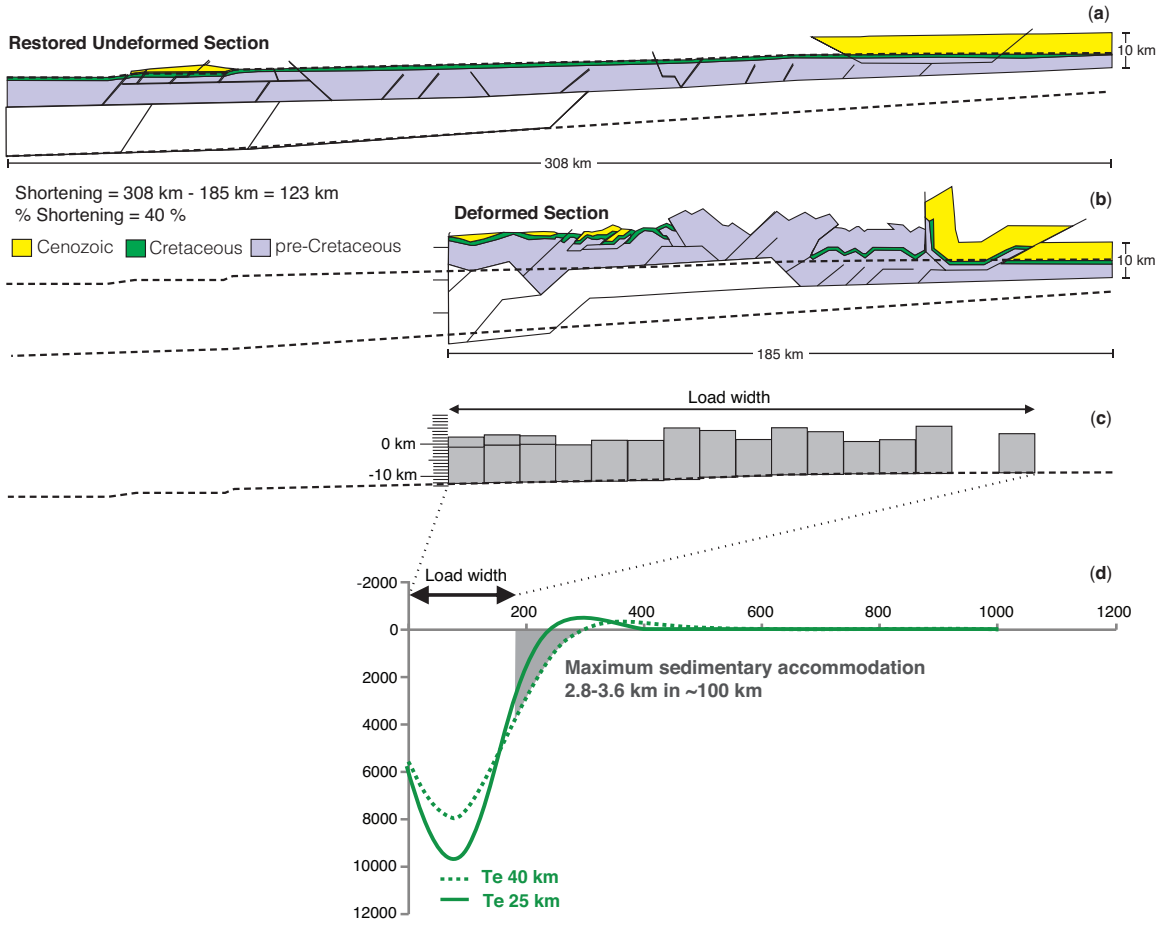

Figure 4. Diagrams illustrating the sequence of steps taken to estimate the flexural component of topography in the region. Firstly, in figures (a) through to (c), the extent of crustal shortening is estimated, and the geometry of the orogenic load reconstructed, based on a balanced cross-section from Gotberg et al. (2010). Then in figure (d) the flexural curves (two green lines) are calculated based on this loading for two different effective elastic thicknesses (Te). The sedimentary accommodation space generated next to the load (i.e. the predicted foredeep), and spanning around 100 km across, is highlighted by the gray shaded triangle.

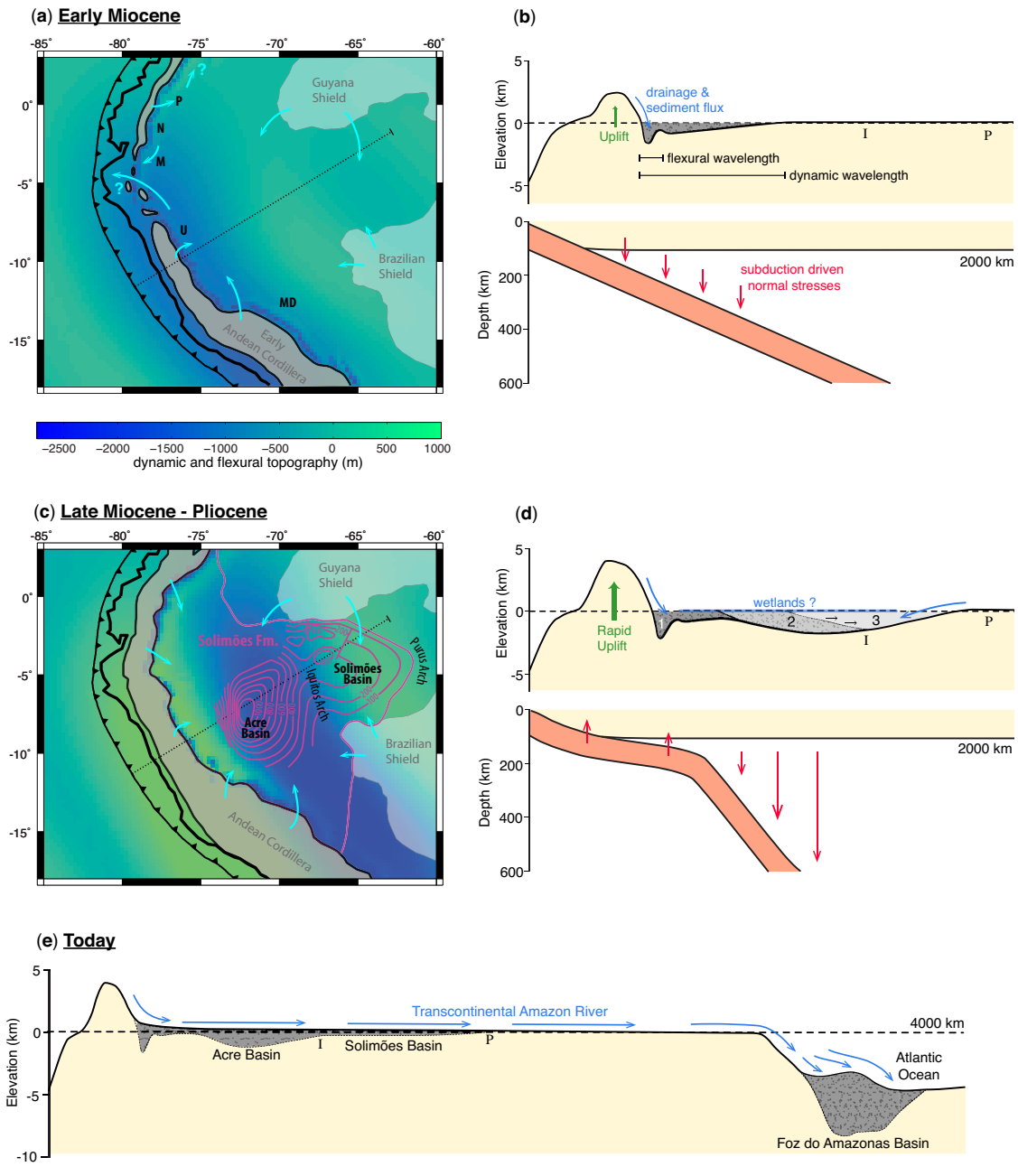

Figure 5. Schematic illustrations demonstrating how a change in subduction style could have driven the topographic and sedimentary evolution of western Amazonia since the Miocene, eventually shaping the present day landscape. Figures (a) and (c) represent maps of the predicted topography from our flexural and dynamic calculations both before and with the arrival of the flat slab. The scale bar for both maps is plotted below figure

908 (a). Turquoise arrows represent drainage directions. The thin dotted line on figures (a)
909 and (c) represents the approximate location of cartoon cross-sections figures (b) and (d)
910 respectively. Gray dotted regions indicate sedimentary infill, with region 1 indicating the
911 oldest deposits and 3 the youngest. The letters I and P on the cross-sections mark the
912 estimated locations of the Iquitos and Purus Arches. Figure (e) is a similar cross-section
913 extending from the trench to the Atlantic Ocean, showing the present day configuration
914 of drainage and the location of the sedimentary deposits that preserve the record of
915 landscape evolution hypothesized in figures (b) and (d).